World Academy of Science, Engineering and Technology
International Journal of Civil and Environmental Engineering
Vol:12, No:3, 2018

Influence of Recycled Concrete Aggregate Content on the Rebar/Concrete Bond Properties through Pull-Out Tests and Acoustic Emission Measurements

L. Chiriatti, H. Hafid, H. R. Mercado-Mendoza, K. L. Apedo, C. Fond, F. Feugeas

Open Science Index, Civil and Environmental Engineering Vol:12, No:3, 2018 publications.waset.org/10008669/pdf

***Abstract*—**Substituting natural aggregate with recycled aggregate coming from concrete demolition represents a promising alternative to face the issues of both the depletion of natural resources and the congestion of waste storage facilities. However, the crushing process of concrete demolition waste, currently in use to produce recycled concrete aggregate, does not allow the complete separation of natural aggregate from a variable amount of adhered mortar. Given the physicochemical characteristics of the latter, the introduction of recycled concrete aggregate into a concrete mix modifies, to a certain extent, both fresh and hardened concrete properties. As a consequence, the behavior of recycled reinforced concrete members could likely be influenced by the specificities of recycled concrete aggregates. Beyond the mechanical properties of concrete, and as a result of the composite character of reinforced concrete, the bond characteristics at the rebar/concrete interface have to be taken into account in an attempt to describe accurately the mechanical response of recycled reinforced concrete members. Hence, a comparative experimental campaign, including 16 pull-out tests, was carried out. Four concrete mixes with different recycled concrete aggregate content were tested. The main mechanical properties (compressive strength, tensile strength, Young's modulus) of each concrete mix were measured through standard procedures. A single 14-mm-diameter ribbed rebar, representative of the diameters commonly used in the domain of civil engineering, was embedded into a 200-mm-side concrete cube. The resulting concrete cover is intended to ensure a pull-out type failure (i.e. exceedance of the rebar/concrete interface shear strength). A pull-out test carried out on the 100% recycled concrete specimen was enriched with exploratory acoustic emission measurements. Acoustic event location was performed by means of eight piezoelectric transducers distributed over the whole surface of the specimen. The resulting map was compared to existing data related to natural aggregate concrete. Damage distribution around the reinforcement and main features of the characteristic bond stress/free-end slip curve appeared to be similar to previous results obtained through comparable studies carried out on natural aggregate concrete. This seems to show that the usual bond mechanism sequence ('chemical adhesion', mechanical interlocking and friction) remains unchanged despite the addition of recycled concrete aggregate. However, the results also suggest that bond efficiency seems somewhat improved through the use of recycled concrete aggregate. This observation appears to be counter-intuitive with regard to the diminution of the main concrete mechanical properties with the recycled concrete aggregate content. As a consequence, the impact of recycled concrete aggregate content on bond characteristics seemingly represents an important factor which should be taken into account and likely to be further explored in order to determine flexural parameters such as deflection or crack distribution.

***Keywords*—**Acoustic emission monitoring, high-bond steel rebar, pull-out test, recycled aggregate concrete.

L. Chiriatti is with the ICube, Université de Strasbourg, CNRS, 2 Rue Boussingault, 67000 Strasbourg, France, IUT Robert Schuman – Génie Civil, 72 Route du Rhin, 67411 Illkirch (corresponding author, phone: +33368858516; e-mail: leon.chiriatti@etu.unistra.fr).

H. R. Mercado-Mendoza, K. L. Apedo and C. Fond are with the ICube, Université de Strasbourg, CNRS, 2 Rue Boussingault, 67000 Strasbourg, France.

F. Feugeas is with the ICube, INSA de Strasbourg, CNRS, 24 Boulevard de la Victoire, 67000 Strasbourg, France.

H. Hafid is with the MISTRAS GROUP SAS, 27 Avenue Magellan, 94370 Sucy-en-Brie, France.

NOMENCLATURE

Symbol	Unit	Quantity
ϕ	m	Rebar nominal diameter
l_0	m	Initial bonded length
s	m	Rebar free-end slip
P	N	Pull-out force
r	%	Fine aggregate replacement rate
R	%	Coarse aggregate replacement rate
ρ_a	kg·m^{-3}	Concrete bulk density
ρ_{rd}	kg·m^{-3}	Aggregate particle density
WA_{24}	%	Water absorption coefficient
k_s	Pa·m^{-1}	Interface shear stiffness
α	%	Fresh concrete air content
h	m	Fresh concrete slump
f_{cm}	Pa	Concrete compressive strength
$f_{ctm,sp}$	Pa	Concrete splitting tensile strength
E_{cm}	Pa	Concrete Young modulus
E_{dyn}	Pa	Concrete dynamic modulus
τ	Pa	Average bond stress
λ_{norm}	variable	Normalized bond parameter
τ_{adh}	Pa	Chemical adhesion strength
τ_{max}	Pa	Bond strength
τ_{res}	Pa	Residual friction stress
A	dB$_{AE}$	Acoustic event amplitude
G	J	Acoustic event absolute energy
G_Σ	J	Cumulated absolute energy

I. INTRODUCTION

CONCRETE is currently the most employed manufactured material in the world. Aggregates, which approximately account for two thirds of the concrete mass, are in most cases extracted from natural deposits. Such level of consumption obviously raises the question of the depletion of this non-renewable resource. In parallel, the increasing production of concrete demolition rubble gives rise to the additional problem of the congestion of waste storage facilities. Recycling concrete demolition rubble for using as aggregate for the manufacture of a second generation of concrete thus

Open Science Index, Civil and Environmental Engineering Vol:12, No:3, 2018 publications.waset.org/10008669/pdf

represents a promising way to address simultaneously both aforementioned problems. A recent study [1] carried out on reinforced concrete beams highlighted that the substitution of natural aggregate (NA) with recycled concrete aggregate (RCA) had an impact on key parameters such as crack distribution and deflection. The composite character of reinforced concrete makes the mechanical response of a member in bending highly dependent on the bond properties between the reinforcement bar (rebar) and the surrounding concrete. Therefore, changes occurring at the rebar/concrete interface, due to the introduction of RCA in the concrete mix, could possibly contribute to such differences.

The RCA replacement rate influence on bond properties has been largely studied over the past ten years. A wide range of experimental setups: pull-out, push-in, beam tests; as well as numerous parameters: rebar diameter, anchorage length, aggregate size, or exposure to high temperatures, have been investigated. Many studies [2]-[6] suggest that the substitution of NA with RCA has no significant impact on bond strength, regardless of the coarse aggregate replacement rate. The substitution of only the NA fine-size-cut with equivalent RCA seems to lead to the same conclusion [7]. However, multiple authors [8], [9] found that an increase in the replacement rate gradually weakens bond properties. On the contrary, some results [10], [11] point out that the larger the coarse aggregate replacement rate, the higher the bond strength. A study [12] dealing with recycled aggregate concrete bond properties after exposure to high temperature confirms the aforementioned trend. Nowadays, there is no clear answer to the impact of RCA replacement rate on rebar/concrete bond properties.

One of the main difficulties encountered in rebar/concrete interaction experimental studies stems from the fact that the interface is deeply embedded into the concrete bulk of the specimen. Nevertheless, obtaining reliable and accurate experimental measurements from this inner region appears to be important in order to analyze the bond-related phenomena taking place therein. Therefore, acoustic emission (AE) monitoring, which exploits the ability of sound to pass through the concrete cover, represents a suitable technique in order to obtain information originating from the whole specimen volume. Watanabe et al. [13] successfully used a single AE sensor on RCA concrete samples which allowed a comparison between the acoustic activity and the load history. Wang et al. [14] used multiple sensors, distributed over the whole surface of a NA concrete pull-out specimen, to determine the location of acoustic events using triangulation. These previous studies confirm that AE monitoring represents a suitable method to investigate both RCA concrete and pull-out specimen.

Considering the conflicting results previously discussed, the target of this work is to enlarge the existing database pertaining to the influence of RCA content on bond properties. A comparative experimental campaign based on pull-out tests was carried out. Four concrete mixes with different RCA content were tested. The pull-out specimen concrete cover was designed to avoid early splitting of the sample so as to compare the response of the different concrete mixes along the whole bond degradation process. These results were enriched with exploratory AE measurements performed on the 100% recycled concrete. The use of multiple sensors allowed us to map the damage distribution in order to compare it to existing data related to NA concrete.

II. Materials and Methods

A. Concrete Compositions

All selected concrete mixes shared a common basis composed of *CEM II/A 42.5N* Portland-blended cement compliant with NF EN 197-1, different proportions of *MC PowerFlow 3140* superplasticizer and *Centrament Retard 370* retarding admixture, and drinking water. Both NA and RCA were graded according to three size cuts ranging from 0 mm to 20 mm. Particle density (ρ_{rd}) and water absorption coefficient (WA_{24}) of the aggregates were determined according to EN 1097-6. Experimental values are summarized in Table I and confirm the trend that RCA generally have lower density and higher absorption coefficient than NA.

TABLE I
Aggregate Properties

Aggregate type	Size cut	ρ_{rd} (kg·m^{-3})	WA_{24} (%)
Natural	0/4	2580	1.08
	4/10	2740	0.89
	6.3/20	2700	0.54
Recycled	0/4	2070	9.86
	4/10	2320	5.85
	10/20	2340	5.41

All details concerning the concrete mixes are listed in Table II. The first concrete mix (rb01), a reference, is exclusively composed of NA.

TABLE II
Concrete Compositions

Ingredient (in kg·m^{-3} **unless specified**)	rb01	rb02	rb03	rb04
Fine aggregate replacement rate (%)	0	0	30	100
Coarse aggregate replacement rate (%)	0	100	30	100
CEM II/A 42.5N cement	270	282	277	326
Betocarb HP OG limestone filler	45	31	31	50
0/4 *Sandrancourt* natural sand	780	806	500	-
0/4 recycled sand	-	-	218	673
4/10 *Givet* natural fine gravel	267	-	171	-
4/10 recycled fine gravel	-	163	145	304
6.3/20 *Givet* natural gravel	820	-	552	-
10/20 recycled gravel	-	701	167	442
MC PowerFlow 3140 superplasticizer	1.31	1.40	1.08	1.18
Centrament Retard 370 retarding admixture	-	-	1.10	2.60
Effective water	180	189	185	199

The second formulation (rb02) is a combination of natural sand and recycled coarse aggregates. The mass substitution of NA by RCA of the third concrete mix (rb03) was set to 30% for both fine and coarse aggregate. The last mixture (rb04) was entirely based on RCA.

B. Rebar Design

A 14-mm nominal diameter crescent-ribbed reinforcement

Open Science Index, Civil and Environmental Engineering Vol:12, No:3, 2018 publications.waset.org/10008669/pdf

was used. Fig. 1 illustrates the rebar rib features and more specifically the different pattern shaped around the reinforcement perimeter. Three groups of ribs can be distinguished:

(a) Alternately inclined crescent-shaped ribs.
(b) A pair of opposite longitudinal ribs.
(c) Regularly inclined crescent-shaped ribs.



Fig. 1 Overview of the steel rebar rib patterns

According to supplier data, values of 500 MPa and 200 GPa were considered for yield strength and Young modulus, respectively. A maximum rib height of 1.0 mm was experimentally measured before casting.

C. Pull-Out Specimen

Four cubic pull-out specimens with a side measuring 200 mm were casted for each concrete mix (cf. Fig. 2). As shown in Fig. 3 (a), an initial anchorage length of 140 mm, representing ten times the rebar nominal diameter, was selected. Such enlarged bonded length (higher than the usual value of five times the rebar diameter) was adopted considering the acoustic event location accuracy estimated to be ±5 mm. However, this bonded length was also limited in order to not exceed the steel yield strength during the rebar pull-out.

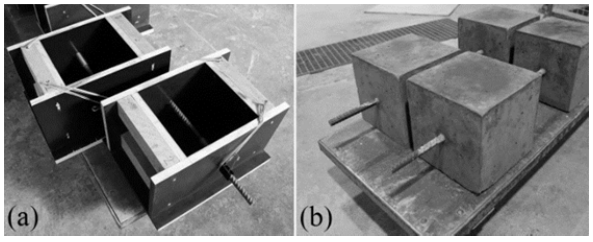


Fig. 2 (a) Formworks, (b) Hardened pull-out specimens

Fig. 3 (a) also illustrates the thin plastic sleeve used as a bond breaker over a length of 60 mm in order to avoid any interaction between the rebar and the concrete cover. Such precaution allows the moving of the anchorage zone away from the contact area between the pull-out specimen base and the testing frame support plate. Any traces of superficial corrosion were removed from the rebar surface with a metallic brush. Any contact with formwork oil was carefully avoided. All samples were casted horizontally, vibrated and cured in a natural indoor environment for 28 days.

D. Experimental Setup

As shown in Fig. 4, a testing frame composed of two 18 mm thick steel plates connected with four 16 mm diameter threaded rods was inserted into an INSTRON 3384 electromechanical press. Pull-out specimens were positioned on the drilled support plate. The lower rebar end was fastened using the press bottom fixed jaw. The upper moving jaw was used to induce a vertical displacement of the whole testing frame. Pull-out is therefore induced by the relative displacement between the ascending concrete cube and the motionless rebar. A force sensor, with a maximum capacity of 150 kN and an accuracy of 0.01 kN, was used to measure the pull-out force (P). The rebar free-end slip (s), defined as the relative displacement between the steel rebar free-end and the surrounding concrete, was measured with a RDP Electronics D5/300AGRA Linear Variable Differential Transformer (L.V.D.T.) with a measuring range of 15 mm and an accuracy of ±1 µm. The press was computer-controlled using INSTRON Bluehill2 software. All pull-out specimens were subjected to a monotonic load, characterized by a constant displacement rate of 0.5 mm/min. A sampling rate of 10 Hz was defined.

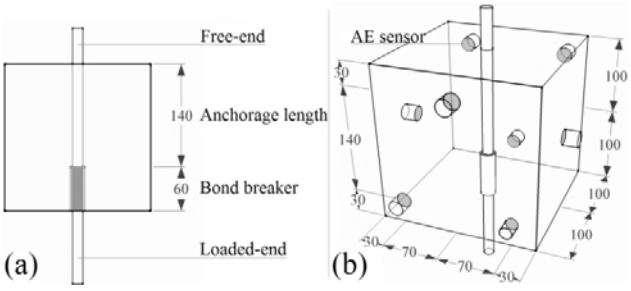


Fig. 3 (a) Interface design, (b) AE sensor distribution

Eight *R15a* piezoelectric sensors, measuring 19 mm in diameter, were distributed over the pull-out specimen envelope according to Fig. 3 (b). The sensor bandwidth, ranging from 75 kHz to 150 kHz, is suitable and currently used for structural concrete damage detection [13], [15]. The *R15a* built-in piezoelectric material was designed for pressure wave emission/reception. All sensors were bonded on the concrete surface using silicone to avoid any absorption due to concrete porosity. Pencil-lead breaks, also called Hsu-Nielsen sources, where used as reproducible AE source in accordance with EN 1330-9 to validate the whole setup. The twofold purpose of such a test was to ensure that all AE sensors were in good contact with the concrete surface and to check the accuracy of the source location setup. Eight *2/4/6* preamplifiers, with a selected gain of 40 dB_{AE}, were used to amplify the sensor output voltage. Low-pass and high-pass filters were respectively set at 20 kHz and 400 kHz in order to remove the audible noise and high frequencies from acquired data. A threshold level of 35 dB_{AE}, intended to separate effective signals from insignificant events, was set.

Open Science Index, Civil and Environmental Engineering Vol:12, No:3, 2018 publications.waset.org/10008669/pdf

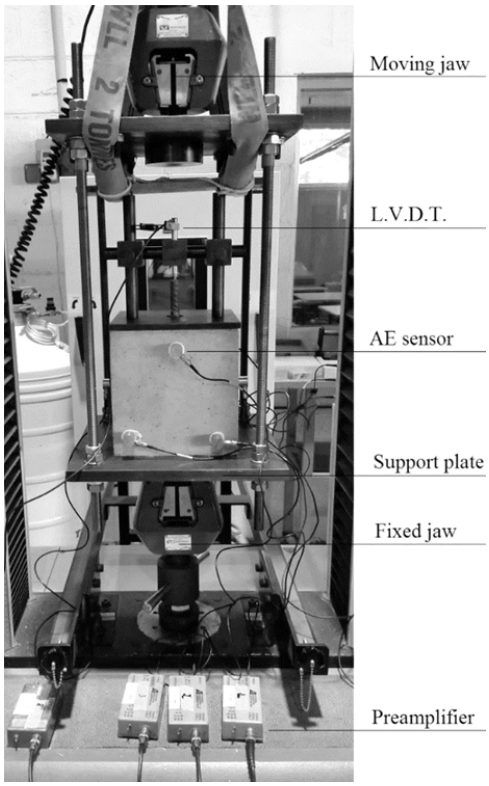


Fig. 4 Experimental setup

Data acquisition was simultaneously performed on all channels using MISTRAS *Express 8* acquisition system. A sample rate of 1 MHz, offering a good compromise between measurement accuracy and dataset size, was defined. Three-dimensional event location, requiring no less than four distinct signal detections, was computed using MISTRAS *AE-WIN 3D-LOC* software. As a consequence, each acoustic event can possibly be described by several electric signals, depending on the number of sensors impacted by the related elastic wave. Conventionally, the acoustic signature recorded by the first impacted sensor is considered as the only one representative of the event. The AE measurement accuracy of ±5 mm (cf. Section II *C*) was estimated taking into account the aforementioned transducer diameter of 19 mm and the potential time-shift related to a sampling rate of 1 MHz.

E. Concrete Properties

The main mechanical properties of each concrete mix are gathered in Table III. Cylinders measuring 11 cm in diameter × 22 cm in height were tested through standard procedures to determine compressive strength (f_{cm} - EN 12390-3), splitting tensile strength ($f_{ctm,sp}$ - EN 12390-6), and Young modulus (E_{cm} - EN 12390-13). Additionally, a PROCEQ *Tico* ultrasonic instrument was used to determine the dynamic modulus (E_{dyn} - EN 12504-4). Air content (α - EN 12350-7) was estimated on fresh concrete as well as workability, determined by means of a slump test (h - EN 206-1). Bulk density (ρ_a) of each hardened concrete sample was also calculated. Compressive strength ranged from 24.8 MPa to 30.1 MPa, without any obvious connection to the RCA content. Splitting tensile strength values of about 2.5 MPa were observed, regardless of the RCA replacement rate. Young's and dynamic modulus, as well as bulk density and air content, seemed to follow the RCA replacement rate trend.

TABLE III
FRESH AND HARDENED CONCRETE PROPERTIES

Quantity	Unit	rb01	rb02	rb03	rb04
Air content (α)	%	1.4	2.5	1.7	3.1
Slump (h)	mm	67	65	113	168
Bulk density (ρ_a)	kg·m^{-3}	**2381**	**2199**	**2279**	**2055**
		± 17	± 15	± 17	± 17
Compressive strength (f_{cm})	MPa	**29.1**	**24.8**	**30.1**	**28.4**
		± 0.9	± 2.0	< 0.1	± 0.6
Splitting tensile strength ($f_{ctm,sp}$)	MPa	**2.6**	**2.6**	**2.5**	**2.4**
		± 0.4	± 0.4	± 0.6	± 0.3
Young modulus (E_{cm})	GPa	**32.6**	**25.2**	**27.6**	**19.3**
		± 0.9	± 0.8	± 1.3	± 2.4
Dynamic modulus (E_{dyn})	GPa	**45.9**	**33.0**	**40.3**	**27.6**
		± 1.5	± 0.6	± 0.8	± 1.4

III. THEORETICAL BACKGROUND

A. Pull-Out Parameters

As shown in Fig. 5, the mechanical response of a pull-out specimen is usually represented through a characteristic curve, expressing the average bond stress (τ) as a function of the rebar free-end slip (s). This curve, obtained from the pull-out tests carried out in this work, corresponds to the general shape described in the literature [16]. The whole specimen behavior is generally divided into three different stages [16], each one related to a specific bond mechanism taking place at the rebar/concrete interface. "Chemical adhesion", restricted to slip values of some micrometers, represents the interface's ability to develop bond stresses without a significant slip. As a consequence, this mechanism is represented by a nearly vertical segment in the τ-s curve. Mechanical interlocking, related to the action of the ribs, bearing against the surrounding concrete, prevails as a bond stress source until slip values of a few millimeters. This hardening phase corresponds to the τ-s curve ascending branch. The post-peak softening behavior, attributed to friction, extends to tens of millimeters before reaching a nearly constant value. The stages in question are characterized by the following parameters, also reported in Fig. 5:

i. Chemical adhesion strength (τ_{adh}): the upper bond stress reached by the interface before the occurrence of a significant slip.
ii. Interface shear stiffness (k_s): the average slope of the practically linear portion of the τ-s curve beyond τ_{adh}.
iii. Bond strength (τ_{max}): the peak stress value reached by the interface throughout the whole shearing process.
iv. Residual friction (τ_{res}): the interface's ultimate bond stress value.

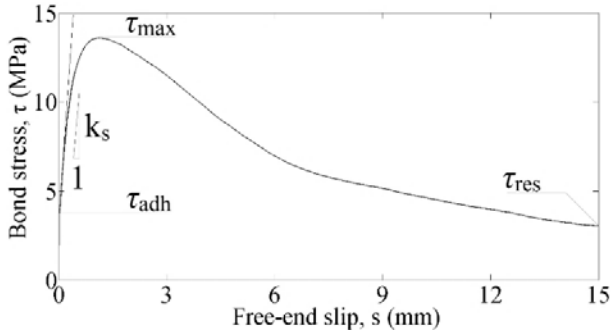


Fig. 5 Typical bond stress/free-end slip curve

Given the significant free-end slip value (s), the relatively limited initial anchorage length (l_0) usually adopted for pull-out specimen needs to be gradually corrected. Therefore, the average bond stress (τ) was calculated, as a function of the pull-out force (P) and the rebar nominal diameter (ϕ), according to (1):

$$\tau = \frac{P}{\pi\phi(l_0 - s)} \quad (1)$$

B. Acoustic Emission Parameters

The piezoelectric effect is exploited by AE transducers to convert mechanical vibrations, induced by damage processes, into an electrical voltage. Fig. 6 illustrates a typical AE signal recorded by an AE sensor. Such waveform can be characterized by a large number of parameters, including its amplitude (A) and its released absolute energy (G).

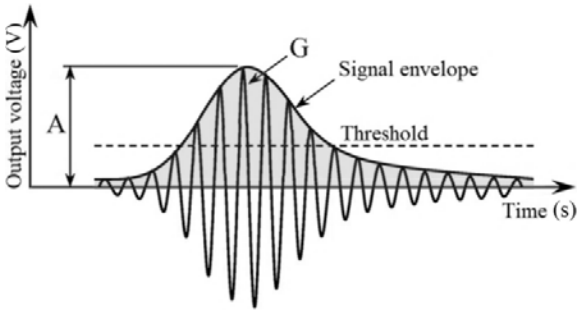


Fig. 6 Typical AE signal

Amplitude, corresponding to the maximum value reached by the electric signal, reflects the damage intensity in connection with the detected event. The voltage level associated with the amplitude is generally converted into acoustic emission decibel (dB_{AE}) according to (2). Absolute energy is proportional to the area under the signal envelope. This parameter, correlated with both event duration and sensor real-time output voltage, is therefore representative of the global magnitude (i.e. extent) of the damage caused by a single event. A threshold level is usually defined in order to separate effective signals from insignificant events. It also sets reasonable limits to the amount of recorded data.

$$A\,(dB_{AE}) = 20 \log\left(\frac{V_{max}}{1\ \mu V}\right) - Gain \quad (2)$$

IV. Results And Discussion

A. Comparison of Bond Mechanical Properties

The four parameters characterizing the bond mechanisms introduced in Section III *A.* were obtained from the experimental results, taking into account the anchorage length rectification according to (1). Average values of each pull-out parameter are listed in Table IV together with the corresponding standard deviations.

TABLE IV
Average Bond Parameters

Quantity	Unit	rb01	rb02	rb03	rb04
Chemical adhesion strength (τ_{adh})	MPa	**1.3**	**2.8**	**3.1**	**1.8**
		± 0.2	± 0.1	± 0.6	± 0.3
Interface shear stiffness (k_s)	MPa·mm^{-1}	**20.9**	**18.9**	**21.4**	**12.2**
		± 5.8	± 2.6	± 3.0	± 6.4
Bond strength (τ_{max})	MPa	**10.4**	**10.1**	**12.0**	**8.4**
		± 0.9	± 0.5	± 0.5	± 0.1
Residual friction (τ_{res})	MPa	**2.7**	**2.3**	**3.1**	**2.0**
		± 0.6	± 0.3	± 1.0	± 0.1
Bond strength slip	mm	**1.72**	**1.11**	**1.55**	**1.55**
		0.26	0.25	0.17	0.15

As done by many authors [2]-[4], [7], all τ-s curves represented in Fig. 7, were normalized by dividing the bond stress dataset of each concrete mix by the square root of the corresponding compressive strength, according to (3). Analogous parameters such as those in Table IV, resulting from normalized curves, are presented in Table V.

TABLE V
Normalized Bond Parameters

Quantity	Unit	rb01	rb02	rb03	rb04
Chemical adhesion strength ($\tau_{adh,norm}$)	MPa$^{0.5}$	0.24	0.57	0.56	0.34
Interface shear stiffness ($k_{s,norm}$)	MPa$^{0.5}$·mm^{-1}	3.87	3.80	3.91	2.28
Bond strength ($\tau_{max,norm}$)	MPa$^{0.5}$	1.92	2.03	2.18	1.57
Residual friction ($\tau_{res,norm}$)	MPa$^{0.5}$	0.49	0.45	0.56	0.37

As far as the specimens tested in this work are concerned, the so-called chemical adhesion mechanism ranges below a free-end slip value of 50 µm, as illustrated in Fig. 8. Within this range, the chemical adhesion strength τ_{adh} was defined as the bond stress corresponding to the inflexion point of the curve. The calculation of τ_{adh} shows that, when taking into account their lesser compressive strengths through the normalization procedure, all RCA mixes performed relatively better than the NA concrete. This observation could likely be associated with the eventual presence of anhydrous cement, into the RCA, which may have been hydrated during the casting. A more compact granular stacking could also partly explain this, regarding the relatively higher proportion of fine particles into recycled sand compared to natural sand.

The hardening window defined in Fig. 9 shows that a nearly linear trend can be identified for every measured τ-s curve. According to this observation, the interface shear stiffness k_s was reckoned to be within a 50-µm to 200-µm free-end slip range. It was found that k_s values of RCA mixes were similar

Open Science Index, Civil and Environmental Engineering Vol:12, No:3, 2018 publications.waset.org/10008669/pdf

Open Science Index, Civil and Environmental Engineering Vol:12, No:3, 2018 publications.waset.org/10008669/pdf

to that of the NA concrete, except for the 100% recycled concrete which showed a significant shear stiffness loss (-40%). Such a result, based on the normalized k_s values, suggests that interface shear stiffness could be somewhat related to the recycled fine aggregate content. The same presumption can be proposed regarding the residual friction response. According to the normalized values and, as shown in Fig. 10, the bond strength of all mixes based on a RCA partial replacement performed better than that of the NA concrete (until +15%). Again, total replacement of NA with RCA led to considerable bond strength reduction (-15%).

$$\lambda_{norm} = \frac{\lambda}{\sqrt{fcm}} \quad (3)$$

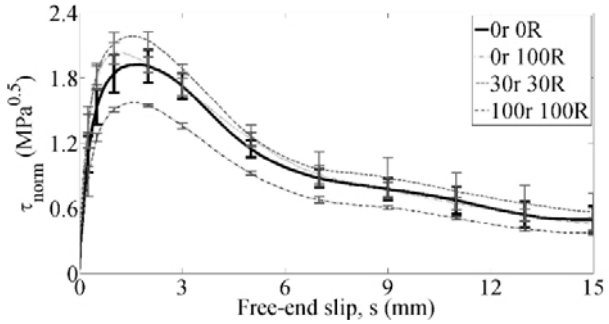


Fig. 7 Normalized bond stress/free-end slip curves

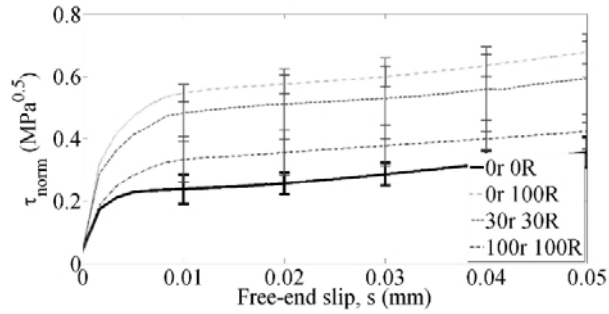


Fig. 8 Chemical adhesion slip range

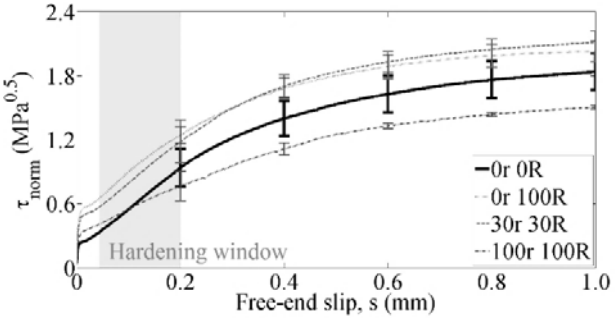


Fig. 9 Interface shear stiffness slip range

B. Analysis of Damage Distribution through AE

AE monitoring provided a database of acoustic events related to damage processes, such as cracking or friction, occurring during the rebar pull-out. 3D location of each event allowed the drawing of a representative map of the damage spread into the surrounding concrete. The acoustic event distribution illustrated in Fig. 11 was extracted using a filter ranging from 70 dB_{AE} to 100 dB_{AE}, corresponding to macro-crack initiation and extension [17]. The resulting map suggests that damage remains mainly located in the vicinity of the rebar.

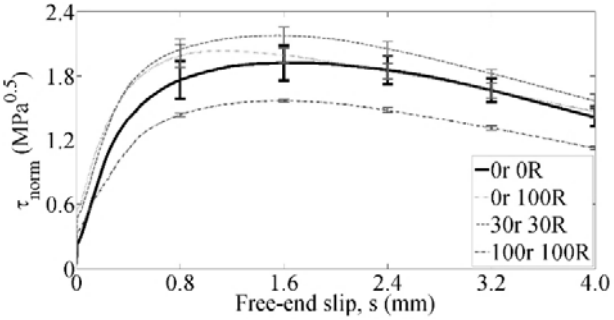


Fig. 10 Bond strength slip range

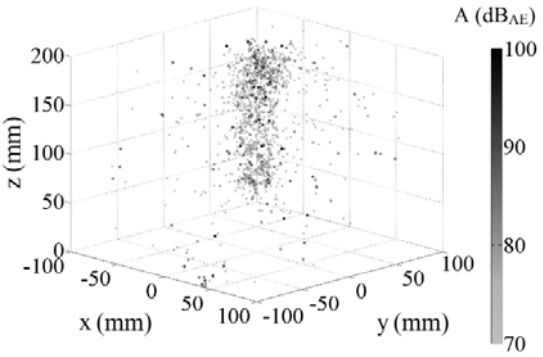


Fig. 11 Overview of the damage spread

Fig. 12 represents the damage intensity as a function of the rebar axis distance, derived on the basis of this dataset. This diagram was obtained by segmenting the cubic concrete volume in 50 concentric cylinders with a 4-mm-step diameter. Damage between two contiguous cylinders was quantified by adding the amplitude of all acoustic events located between them. The 50 resulting values where normalized using the overall sum of the amplitudes which correspond to the whole concrete volume. Damage scope seems to range essentially from the rebar/concrete interface to a distance close to the maximum aggregate size (20 mm). It also appears practically nullified beyond twice a comparable distance from the interface. The aforementioned approach was adapted in order to evaluate the damage intensity profile based on vertical radial plans circling around the rebar. For this purpose, the cubic concrete volume was this time segmented in 45 rotating slices. The logic for quantifying the damage intensity between two contiguous slices remained unchanged. Fig. 13 illustrates the resulting chart and highlights a strong connection between rib height and damage distribution.

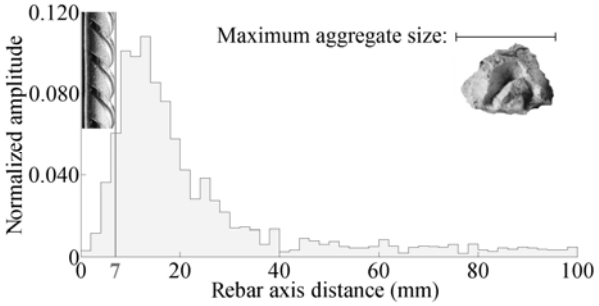


Fig. 12 Damage intensity as a function of the rebar axis distance

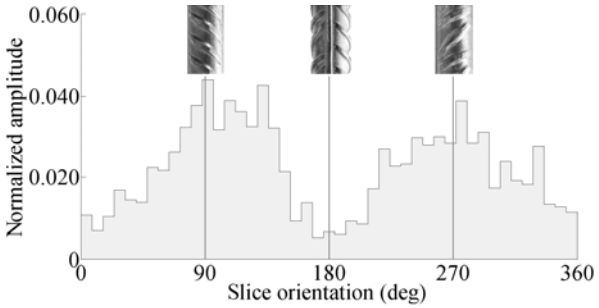


Fig. 13 Distribution of damage intensity around the rebar perimeter

Cumulated absolute energy (G_Σ) was calculated as the sum of the absolute energy which corresponds to the overall events registered throughout the rebar pull-out. G_Σ, which reflects the acoustic activity induced by the reinforcement pull-out, was plotted as a function of the rebar free-end slip (cf. Fig. 14). Despite several discontinuities related to particularly dynamic events, a linear trend can clearly be ascertained. This appears to reveal a close connection between free-end slip and damage growth, summarized by (4).

$$\frac{\Delta G_\Sigma}{\Delta s} \approx C^{ste} \quad (4)$$

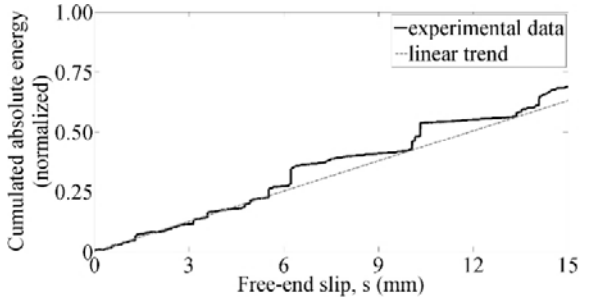


Fig. 14 Damage growth as a function of the rebar free-end slip

V. Conclusion

The following principal conclusions can be drawn from this study:

1) The usual bond mechanism sequence ("chemical adhesion", mechanical interlocking, and friction.) does not seemed impacted by partial or total substitution of NA with RCA.
2) Bond parameters' normalization highlighted that the introduction of coarse RCA seems to improve, or at least maintain, the main bond properties despite generally lower concrete characteristics.
3) Pull-out parameters appeared to be sensitive to the introduction of recycled sand, which seemingly tends to weaken bond properties. This supports the idea that fine aggregates play a particular role.
4) Damage derived from rebar/concrete interaction remained confined to the rebar vicinity and seemed highly dependent on the rib shape, which suggests the development of damage clusters.
5) The free-end slip appeared to be proportional to the cumulated absolute energy, representative of the overall damage magnitude.

The composite character of reinforced concrete entails a close connection between the mechanical response of a reinforced concrete member and the bond properties of the rebar/concrete interface. The bond parameters' specificities, related to the introduction of RCA into the concrete mix, could likely account for the particular behaviors observed on recycled reinforced concrete beams in terms of deflection and crack distribution.

Acknowledgment

The ICube laboratory Civil Engineering team would like thank MISTRAS GROUP for its valuable contribution to the acoustic emission measurements discussed in the present paper.

References

[1] M. Arezoumandi, A. Smith, J. S. Volz, and K. H. Khayat, "An experimental study on flexural strength of reinforced concrete beams with 100% recycled concrete aggregate," Engineering Structures, vol. 88, pp. 154–162, Apr. 2015.
[2] S.-W. Kim and H.-D. Yun, "Influence of recycled coarse aggregates on the bond behavior of deformed bars in concrete," Engineering Structures, vol. 48, pp. 133–143, Mar. 2013.
[3] M. Breccolotti and A. L. Materazzi, "Structural reliability of bonding between steel rebars and recycled aggregate concrete," Construction and Building Materials, vol. 47, pp. 927–934, Oct. 2013.
[4] S. Moallemi Pour and M. S. Alam, "Investigation of Compressive Bond Behavior of Steel Rebar Embedded in Concrete with Partial Recycled Aggregate Replacement," Structures, vol. 7, pp. 153–164, Aug. 2016.
[5] I. Fernandez, M. Etxeberria, and A. R. Marí, "Ultimate bond strength assessment of uncorroded and corroded reinforced recycled aggregate concretes," Construction and Building Materials, vol. 111, pp. 543–555, May 2016.
[6] M. J. Robert Prince, G. Gaurav, and B. Singh, "Splice strength of deformed steel bars embedded in recycled aggregate concrete," Structures, vol. 10, pp. 130–138, May 2017.
[7] S.-W. Kim and H.-D. Yun, "Evaluation of the bond behavior of steel reinforcing bars in recycled fine aggregate concrete," Cement and Concrete Composites, vol. 46, pp. 8–18, Feb. 2014.
[8] H. Yang, Z. Deng, and J. M. Ingham, "Bond position function between corroded reinforcement and recycled aggregate concrete using beam tests," Construction and Building Materials, vol. 127, pp. 518–526, Nov. 2016.
[9] K. Pandurangan, A. Dayanithy, and S. Om Prakash, "Influence of treatment methods on the bond strength of recycled aggregate concrete," Construction and Building Materials, vol. 120, pp. 212–221, Sep. 2016.
[10] J. Xiao and H. Falkner, "Bond behaviour between recycled aggregate concrete and steel rebars," Construction and Building Materials, vol. 21, no. 2, pp. 395–401, Feb. 2007.
[11] M. John Robert Prince and B. Singh, "Bond behaviour of deformed steel bars embedded in recycled aggregate concrete," Construction and Building Materials, vol. 49, pp. 852–862, Dec. 2013.

Open Science Index, Civil and Environmental Engineering Vol:12, No:3, 2018 publications.waset.org/10008669/pdf

[12] H. Yang, W. Lan, Y. Qin, and J. Wang, "Evaluation of bond performance between deformed bars and recycled aggregate concrete after high temperatures exposure," Construction and Building Materials, vol. 112, pp. 885–891, Jun. 2016.
[13] T. Watanabe, S. Nishibata, C. Hashimoto, and M. Ohtsu, "Compressive failure in concrete of recycled aggregate by acoustic emission," Construction and Building Materials, vol. 21, no. 3, pp. 470–476, Mar. 2007.
[14] L. Wang, J. Yi, H. Xia, and L. Fan, "Experimental study of a pull-out test of corroded steel and concrete using the acoustic emission monitoring method," Construction and Building Materials, vol. 122, pp. 163–170, Sep. 2016.
[15] J. Saliba, A. Loukili, F. Grondin, and J.-P. Regoin, "Experimental study of creep-damage coupling in concrete by acoustic emission technique," Materials and Structures, vol. 45, no. 9, pp. 1389–1401, Sep. 2012.
[16] Fédération Internationale du Béton (FIB), "Bond of reinforcement in concrete: state-of-art report," International Federation for Structural Concrete, pp. 3-5, 2000.
[17] Rao, GM Nagaraja, C. R. L. Murthy, and N. M. Raju. "Characterization of micro and macro cracks in rocks by acoustic emission," Acoustic Emission: Standards and Technology Update, ASTM International, 1999.

Open Science Index, Civil and Environmental Engineering Vol:12, No:3, 2018 publications.waset.org/10008669/pdf